The Effect of Molecular Shape on the Thermotropic Liquid Crystal Behavior of Monolauroylated Amino Acid Glyceride Conjugates

M. Carmen Morán,*,† A. Pinazo,† P. Clapés,‡ M. Rosa Infante,† and R. Pons†

Departament de Tecnologia de Tensioactius, Institut d'Investigacions Químiques i Ambientals de Barcelona-CSIC, Jordi Girona, 18−26, 08034 Barcelona, Spain, and Departament Química de Pèptids i Proteïnes, Institut d'Investigacions Químiques i Ambientals de Barcelona-CSIC, Jordi Girona, 18-26, 08034 Barcelona, Spain

Received: June 9, 2005; In Final Form: October 7, 2005

Monoacylglycerol amino acid conjugates constitute a novel class of specific biocompatible surfactants that can be considered analogues to partial glycerides and lysophospholipids. They consist of one aliphatic chain and one polar head, i.e., the amino acid, linked through a glycerol moiety. In a previous work, we synthesized monolauroylated amino acid glyceride conjugates, 1-*O*-lauroyl-*rac*-glycero-3-*O*-(N^{α}-acetyl-L-amino acid), changing the amino acid headgroup systematically: arginine (compound **2**), aspartic acid (compound **3**), glutamic acid (compound **4**), asparagine (compound **5**), glutamine (compound **6**), and tyrosine (compound **7**), to elucidate the structure−properties relationship governing the occurrence of their polymorphism. The thermotropism of the new compounds was measured with polarizing light microscopy, differential scanning calorimetry, and X-ray diffraction and compared with the classical monoglyceride *rac*-1-lauroylglycerol (compound **1**). The experiments were performed for a sequence of heating, cooling, and reheating scans. The results showed that compounds **1**−**6** exhibit a thermotropic smectic phase. As a consequence, the substitution of the polar head did not engender any curvature into the system, which might lead to the formation of cubic or columnar phases. Interestingly, liquid crystalline phases were not found in the case of compound **7**. Small-angle X-ray diffraction data in the gel phase revealed that the substitution of the polar head by the different amino acid structures did not modify significantly the lamellar repeat distance relative to that of the reference one. The observed area per molecule, however, was larger for the new compounds. Consequently, interdigitation was promoted in compounds **2**−**7**. The diffraction patterns were analyzed in terms of electron density profiles, using a modified Caillé theory plus a Gaussian electron density representation (MCG method) on X-ray diffraction data.

1. Introduction

Because of their importance as major components of biological membranes, the self-organization of lipids has gained great scientific interest. However, less attention has been directed toward understanding the behavior of the minor lipid components and how their function influences membrane properties. Lysophospatidylcholines are natural constituents of many biological membranes. They usually occur in small amounts but have nevertheless attracted much interest, mainly because of their membrane-perturbing properties.[1−4]

One approach to systematic studies uses chemically modified lipids,[5−7] providing information about competitive interactions between hydrophilic and hydrophobic moieties of the amphiphiles. The main goal of such experiments is to get a better understanding of the relation between chemical structure and lipid polymorphism.

Understanding the relationships structure/function requires the study of the behavior of these lysophospholipids at the molecular level. A relatively important, and little studied, issue of lysophospholipids is how they behave in a lipid bilayer. Little is known as to the structure, whether they can undergo similar phase transitions as those observed in other lipids, and how the structure of lysophospholipid molecules affects global lipid bilayer structure. While the physical properties of phospholipids have been studied extensively, the physical behavior of lysophospholipids is only now being studied in detail.[8−10]

Monoacylglycerol amino acid conjugates constitute a novel class of specific biocompatible surfactants, which can be considered analogues to partial glycerides and phospholipids. They consist of one aliphatic chain and one polar head, i.e., the amino acid, linked through a glycerol moiety. With the aim of producing mimetic compounds of phospholipid molecules with higher solubility and antimicrobial activity, our group has recently synthesized monoacylglycerol amino acid-based surfactants (Figure 1) by using enzymatic and chemical processes.[11−13] We have recently synthesized monolauroylated amino acid glyceride conjugates and changed the amino acid headgroup systematically to elucidate the structure−property relationship governing the occurrence of the above-mentioned polymorphism. The possibility of introducing different ionic groups, that is, selecting the amino acid, increases the potential of application in pharmaceutical and food formulations.

As in conventional glycerides,[14] spontaneous intramolecular acyl-migration reactions are observed for the lauroyl and aminoacyl moeities of the glycerol backbone,[11] and both possible regioisomers are obtained: 1-*O*-lauroyl-*rac*-glycero-3-*O*-(N^{α}-

* Author to whom correspondence should be addressed. E-mail: mmbste@cid.csic.es.

† Departament de Tecnologia de Tensioactius.

‡ Departament Química de Pèptids i Proteïnes.

10.1021/jp053093l CCC: $30.25
Published on Web 11/05/2005

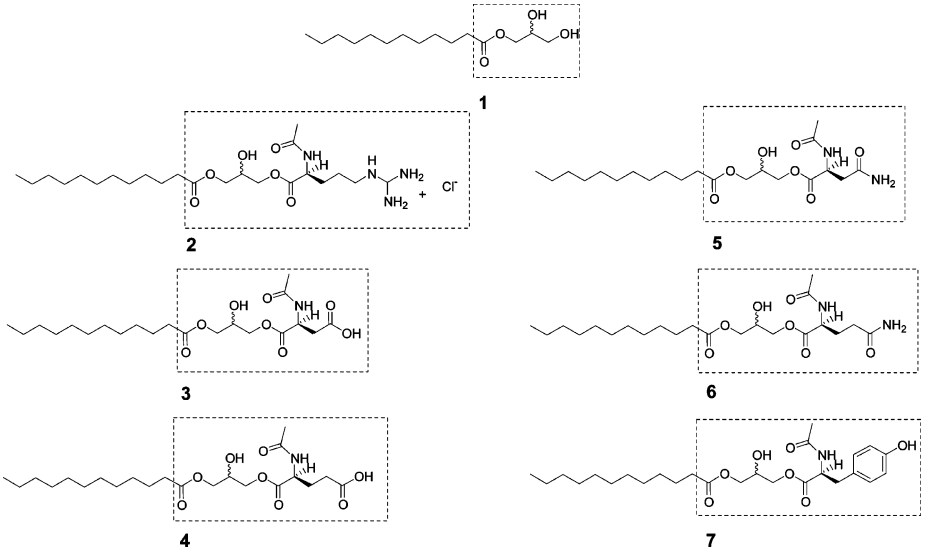

Figure 1. Chemical structure of 1-*O*-lauroyl-*rac*-glycerol (**1**) and the 1-*O*-lauroyl-*rac*-glycero-3-*O*-(N^{α}-acetyl-L-amino acid) derivatives (**2**−**7**) used in this study. The dotted section shows the corresponding polar group in each compound.

acetyl-L-amino acid) and 1(2)-*O*-lauroyl-*rac*-glycero-2(3)-*O*-(N^{α}-acetyl-L-amino acid).

On the other hand, it is known that monoacylgycerols are amphipathic molecules of importance in both industrial and biological contexts. In the food industry, racemic mixtures of 1- and 3-acylglycerols and 2-acylglycerol are employed as emulsifying agents and also emulsifiers and detergents. In biology, monoacylglycerols are important products and intermediates of many lipid reactions.[15]

According to Malkin and Shurbagy,[16] the spacings of racemic mixtures of 1- and 3-acyl-*sn*-glycerols from decanoyl to stearoyl in the α- and β-phases are similar with respect to the enantiomeric ones.[15] Larsson[17] also showed that, although differences in crystal form may exist between the optically active and racemic compounds, the tilt angle was always the same from the bilayer plane. More recently, Persson[18] has shown that racemic mono-*O*-alkylglycerols exhibit very similar phase behavior to that of the optically pure monoacylglycerols. These results suggest that the phase behavior of our racemic mixtures of monolauroyl amino acid conjugates would be similar to that of enantiomeric compounds.

With the aim to elucidate the influence of the molecular structure on the thermotropic liquid crystal behavior and bilayer structure of racemic mixtures of monolauroylated amino acid glyceride conjugates in the dry state, a systematic study of the new monolauroylated amino acid conjugates was performed. The thermotropism was measured with polarizing light microscopy, differential scanning calorimetry, and X-ray diffraction. The diffraction patterns have been analyzed in terms of electron density profiles by using a MCG method on X-ray diffraction data.[19] Information gained from such studies is necessary for the appropriate design and application involving these compounds. Future studies will examine the interaction of these molecules with water and in combination with conventional lipids.

2. Experimental Section

2.1. Materials. *rac*-1-Lauroylglycerol (compound **1** in Figure 1) (>99.0%, monoglyceride standard) was purchased from Fluka. The lauroyl amino acid-based surfactants (compounds **2**−**7** in Figure 1) were synthesized in our lab according to the methods described before.[11,12] Analysis of the synthesized products by ^{1}H NMR spectroscopy showed the presence of a major product, namely 1-*O*-lauroyl-*rac*-glycero-3-*O*-(N^{α}-acetyl-L-amino acid) (Figure 1) and a minor one corresponding to the acylation of the secondary hydroxy group of the glycerol moiety (2-*O*-lauroyl-*rac*-glycero-3-*O*-(N^{α}-acetyl-L-amino acid). The proportion of the regioisomers in the products was calculated by ^{1}H NMR spectroscopy and is summarized in Table 1. The content of the 2,3-regioisomer (1,3: 20%) was lower than in conventional glycerides (40%),[14] with the exception of the tyrosine derivative, for which the content of the 2,3-regioisomer was 63%. All the compounds, as the commercial compound *rac*-1-lauroylglycerol, were mixtures (approximately 50:50) of diastereoisomers.

TABLE 1: Content of 2,3-Regioisomers in the Synthesized Monolauroylated Compounds

	compound						
	1	2	3	4	5	6	7
2,3-regioisomer (%)	0	21	20	18	20	16	63

2.2. Methods. *2.2.1. Polarized light microscopy.* A microscope (Reichert Polyvar 2) equipped with a heating stage was used to observe the texture of samples during the heating process. Samples kept between cover slides were heated from 20 to 100 °C and their changes were monitored. Between heating scans, the samples were allowed to cool to 20 °C while keeping them in a desiccator to avoid hydration. The samples were illuminated with linearly polarized light and analyzed through a crossed polarizer. Images at different critical temperatures were captured by using a video camera and a PC running Leica IM 500 software.

2.2.2. Differential Scanning Calorimetry (DSC). DSC measurements were carried out by using a 821^e DSC (Mettler Toledo) equipped with a cryostat cooling system. Data were treated by using the STAR Software (Mettler Toledo). A flow rate of 50 mL/min of nitrogen was used in the DSC cell. Samples (3−4 μg) of the dry lipids were scanned by using hermetically sealed aluminum pans of 40 μL volume (Mettler Toledo). Indium was used as a standard to calibrate the DSC temperature and enthalpic scales. TGA was used to check for product decomposition on heating above the melting point. The analyses showed no sample destruction within the investigated temperature range. Some weight loss during the heating can be

attributed to slight hydration of the products during sample preparation (around 0.5%).

2.2.3. X-ray Scattering (SAXS). Small-angle X-ray scattering (SAXS) measurements were carried out by using a Kratky compact camera of small angle (Hecus X-ray Systems, Graz) coupled to a Siemens KF 760 (3KW) generator. Nickel-filtered radiation with wavelength corresponding to the Cu Kα line (1.542 Å) was used. The linear detector was a PSD-OED 50 M-Braun, and the temperature controller was a Peltier KPR (Anton Paar, Graz). X-ray diffraction samples were inserted into a 1.0 mm quartz capillary or between two Mylar sheets with a 1 mm separation, depending of the texture of the samples.

The temperature protocol for the SAXS data included one heating scan, one cooling scan, and one reheating scan. However, only in the heating and reheating scans was SAXS data recorded. Therefore, the SAXS data corresponded to known thermal conditions. On the first scan, samples were heated from 0 to 70 °C with the Peltier system (0−70 °C) in 32 temperature steps. Each step consisted of setting the temperature of the specimen stage, waiting for 5 min for thermal equilibration, and then the diffraction pattern was recorded during 5 min. If the melting point of the compound was over 70 °C, the sample was removed and placed in a separate heating system running at higher temperatures (25−300 °C). After the maximum temperature was reached, the sample equilibrates down to room temperature without temperature control. The equilibration time was around 18−24 h. The next scan took the room-temperature sample to 0 °C for 10 min, then the reheating scan was recorded. In the case of compounds with transitions over 25 °C, the heating and reheating scans were carried out in the high-temperature system (25−300 °C).

The SAXS scattering curves are shown as a function of the scattering vector modulus,

$$q = \frac{4\pi}{\lambda} \sin \theta/2 \tag{1}$$

where θ is the scattering angle, and λ the wavelength of the radiation. The q values with our setup ranged from 0.1 to 6.0 nm^{-1}. By using Bragg's law with $d = 2\pi n/q$ and n the order of reflection, the corresponding distances were between 60.0 and 1.1 nm.

The SAXS method used to resolve periodic structures in the complexes is essentially X-ray powder diffraction. In this technique, the sample is assumed to contain small crystallites at random orientations. Thus, when monochromatic X-rays are collimated on the sample, a sharp maximum must appear in the scattered intensity whenever the length of the scattering vector q matches any of the reciprocal lattice vectors. If a sufficient number of these peaks are observed, their relative positions on the q-axis unambiguously reveal the periodicity of the structure. The measured spacing d is accurate to better than 0.03 nm, and the temperature of the X-ray specimen stage was controlled to better than ± 0.5 °C.

Further information has been derived by the analysis of the diffraction patterns in terms of electron density profiles. The profiles were derived by MCG methods[19] for gel phase patterns.

It is known that the intensity scattered from a finite stack of unoriented bilayers is described by

$$I(q) \propto \frac{\langle |f(q)|^2 s(q) \rangle}{q^2} \tag{2}$$

where q is the absolute value of the scattering vector (see eq 1), $f(q)$ the form factor, and $s(q)$ the structure factor. The form factor characterizes the electron density distribution and is given in the case of a layered structure by the Fourier transform

$$f(q) = \int \rho(z) \exp(iqz) \mathrm{d}z \tag{3}$$

of the electron density profile ρ along the z axis.

The MCG method analyzes both Bragg peaks and diffuse scattering. This method considers scattered intensities in the full 2θ range. Therefore, one can then retrieve structural information, even if only a few orders of diffraction are observed. The MCG uses a Gaussian description of the electron density, setting two symmetric Gaussian to describe the polar heads. A further Gaussian is centered at the center of the bilayer, describing the low-electron-density methyl terminal hydrocarbon chains. The form factor calculated from the electron density profile model is coupled to a structure factor given by the modified Caillé theory. This coupled form−structure factor can be calculated analytically and is a continuous function of q, which allows for a global description of the full small-angle scattering range.

The structure factor in this model takes the form:

$$\langle s(q) \rangle = S(q) = N + 2\sum_{N-1}^{k=1} (N-k) \cos(kpd) e N^{-(d/2\pi)^2 q^2 \eta_1 \gamma} (\pi k)^{-(d/2\pi)^2 q \eta_1} \tag{4}$$

where the mean number of coherent scattering bilayers in the stack is denoted as N, *and* γ is Euler's constant. The Caillé parameter η_1 involves both the bending modulus of lipid bilayers and the bulk modulus for compression.

In the MCG model, an additional diffuse scattering contribution was considered by accounting for uncorrelated bilayers and unilamellar vesicles. We will see that, in our case, in dry samples, this diffuse scattering is negligible.

The corresponding electron density profile is calculated by a summation of two Gaussian, each representing the polar headgroup and the methyl terminus, respectively

$$\rho(z) = \rho_{CH_2} + \bar{\rho}_H \left[\exp\left(-\frac{(z - z_H)^2}{2\sigma_H^2} \right) + \exp\left(-\frac{(z + z_H)^2}{2\sigma_H^2} \right) \right] + \bar{\rho}_c \exp\left(-\frac{z^2}{2\sigma_C^2} \right) \tag{5}$$

The position of the Gaussian peak is at z_i ((i) = H,C; z_C = 0), with a standard deviation of σ_i. The fit has been performed by minimizing χ^2 using statistical weighing. A flat background has been subtraction calculated as the mean intensity between 0.4 and 0.46 $Å^{-1}$. This fit has been performed directly on the instrumentally smeared scattering patterns. The calculated pattern has been smeared for length and width of the line-shaped X-ray beam. Both profiles have been experimentally determined under the same experimental conditions. This is more convenient than fitting a desmeared profile because the desmearing procedure introduces artifacts when peaks are present.

By using the MCG method, structural parameters can be derived from simple geometric relationships, determining the area per molecule (A), the hydrocarbon chain length (d_C), and the headgroup size (d_H). The area per molecule was determined according to:

$$A = \frac{1}{\rho_{CH_2}(\tilde{\rho}_r - 1)} \left(\frac{\tilde{\rho}_r n_C^e}{d_C} - \frac{n_H^e}{d_H} \right) \tag{6}$$

TABLE 2: Transition Temperatures and Observed Phases for the Compound 1−7 Values Determined with Polarized Light Thermal Microscopy[a]

compound	initial phase	transition temperature (°C)	phase	transition temperature (°C)	phase
1	Cr	65	Sm	160	I
2	Cr	70	Sm	80	I
3	Cr	50	Sm	75	I
4	Cr	43	Sm	170	I
5	Cr	50	Sm	170	I
6	Cr	75	Sm	100	I
7	V				

[a] Cr, crystalline; Sm, smectic; V, viscous no-birefringent; I, isotropic melting.

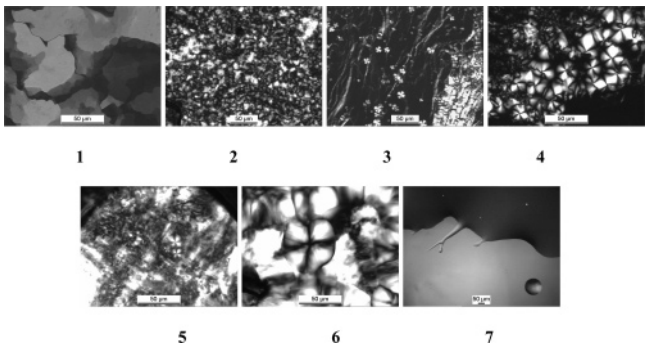

Figure 2. Representative optical polarized micrographs displayed by compounds **1**−**7** upon the first heating step: **1**, mosaic structure in the smectic phase (80 °C); **2**, mosaic structure (80 °C); **3**, oily streaks and positive units (50 °C); **4**, negative units and fanlike structure (75 °C); **5**, positive units (60 °C); **6**, positive units (80 °C); **7**, viscous no-birefrigent phase (25 °C). In the case of compound **7**, the polarizer is not crossed at 90° so that the texture becomes visible.

where $\rho_r \cong \rho_H/\rho_C$ and n_C^e is the number of hydrocarbon electrons and n_H^e the number of headgroup electrons, respectively. Because in our fit an arbitrary value for the intensity scaling was used, it was possible to further bind the hydrophilic electronic density to the rest of parameters. In fact, this was necessary to achieve a reasonable minimization path. Therefore, we used the relationships:

$$d_c = z_H - \frac{(d/2 - z_H)}{2} \tag{7}$$

for the hydrocarbon chain length d_C and the headgroup size d_H

$$d_H = \frac{d}{2} - d_C \tag{8}$$

and

$$\rho_H = \rho_C \frac{(V_C \rho_{CH_2} - n_C)}{V_C \rho_{CH_2} - n_H d_C/(d/2 - d_C)} \tag{9}$$

Note that eqs 6 and 9 differ slightly from those used in the literature[19] because no water is present.

3. Results and Discussion

3.1. Polarized Light Microscopy (PLM). The thermotropic liquid crystal properties of compounds **1**−**7** were determined by thermal polarized microscopy, and the obtained results are given in Table 2 and Figure 2. No clearly defined melting point for the transition from the solid state to the liquid crystal phase could be identified because the paramorphotic defect texture of the crystal was retained into the liquid crystal phase, and consequently, the materials appeared to change from a solid to a soft crystal and only then become liquid.

If we try to relate the chemical structure with the observed transition temperatures, no clear logic seems to apply. In the arginine derivative (**2**), one hydroxyl group of the glycerol moiety on the monoacylglycerol (compound **1**) is replaced by the more polar amino acid arginine. This amino acid group would act more efficiently in the hydrogen bond network. However, the clearing temperature of **2** was lower relative to that of **1**. Considering the coexistence of the two possible regiosiomers in equilibrium (Table 1), this behavior would be mainly related with the entropy of the mixture. The replacement by an aspartic acid derivative (**3**) showed a similar reduction in the clearing temperature. The glutamic derivative (**4**), with one more methylene group in the side chain to that of the aspartic acid derivative (**3**), exhibited a comparable clearing temperature to **1**.

In the nonionic compounds **5** and **6**, the carboxylic groups of the side chain of **3** and **4** were replaced with an amide group. Thus, the clearing temperature of **6** is lower relative to that of **4**. Unexpectedly, the clearing temperature of **5** increased.

Compound **7** is oil at room temperature and did not show melting point. In this case, the number of hydroxyl groups remained constant with respect to the dodecyl glycerol. This compound, however, did not show any liquid crystalline behavior. The introduction of the tyrosine residue may shift the ratio between the polar and nonpolar parts in the mixture toward the polar part.

3.2. DSC Studies. To study the thermotropic mesophase formation in more detail, DSC studies on the new compounds **2**−**7** and compound **1** were carried out. Measurements were conducted with an identical heating and cooling rate (5 °C/min) over a temperature ranging from −30 to 140 °C. Figure 3 shows the obtained thermograms. The transition temperatures corresponding to phases changes observed under the microscope were confirmed by using differential scanning calorimetry (DSC). The DSC thermogram for compound **1** shows the general phase behavior described for monoglycerides.[15,20] In the initial heating, the transition observed corresponds to the melting of the more stable polymorphic β-form obtained from solvent of crystallization. The values of temperature and enthalpy of this transition (61.13 °C and 12.65 kcal/mol, respectively) are in good agreement with the ones described in the literature.[15] On cooling from the isotropic liquid, the compound crystallized to an unstable α-phase. On reheating, this α-phase melted (35.89 °C) and crystallized to the more stable β-form (45.37 °C), which melted to the isotropic liquid (53.00 °C).

Because of the similarity between the synthesized compounds (**2**−**7**) and the standard one (**1**), the same nomenclature of polymorphs used in partial glycerides will be adopted. Only **6** exhibited one exothermic peak, which corresponds to the crystallization from the melted α-form to a β-form. The almost nondetectable endotermic melting of α-form compared with the high endothermic melting of β-form suggested that a high portion of the transformation between the two polymorphs occurred in the solid state. In compound **6**, higher melting temperature of β-forms than in **1** was observed. This behavior suggests that the introduction of the glutamine moiety in the molecule may improve the stability of their β-form structure. Nevertheless, identical values in the transition temperature from the α- to the β-form for **1** and **6** were observed, suggesting that the stability of the α-form of both compounds was similar.

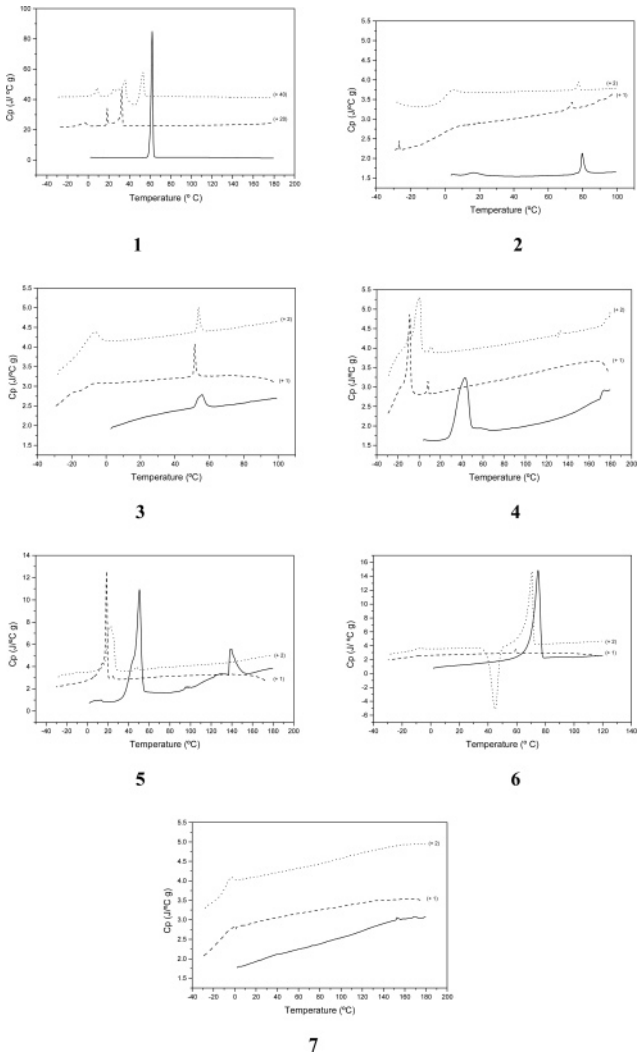

Figure 3. DSC thermograms of compounds **1**−**7**. The experiments were performed for a sequence of heating, cooling, and reheating scans (from bottom to top). Cooling and reheating curves were shifted for clarity.

The thermal behavior of **2** and **3** was simpler. For both compounds, in the initial heating, the β-form underwent a single poor energetic transition to the isotropic liquid. On cooling from the isotropic liquid, both compounds crystallized to the unstable α-phase, which melts at a temperature very close to that of the melting temperature of the β-phase. Moreover, the melting temperature and enthalpy of the transition from the α-phase to the isotropic liquid were in both cases always less than those of the β-phase to isotropic liquid transition.

In the initial heating, the β-form of **4** and **5** underwent a single broad transition to the isotropic liquid. On cooling from the isotropic liquid, two exothermic transitions were observed: one small exothermic corresponding to the crystallization of the α-phase and a second crystallization to a more stable β- or β'-phases. Subsequent reheating showed the transformation between these β- or β'-phases to the α-phase and then the melting of the α-phase. Compound **7** did not show any transitions in the range of temperature studied. The presence of the tyrosine structure in the polar head could favor the mixture between the hydrocarbon chains and the polar group, thus producing a decrease of the freezing point. The small transition observed around 0 °C in the reheating scan is of unknown nature. Observation of the sample between crossed polarizers at −20 °C did not show any birrefringence.

TABLE 3: Phase Transition Temperatures (°C) and Enthalpies (kcal/mol) Derived from the DSC Curves of the Monolauroylated Amino Acid Conjugates (2−7)

compound	heating	cooling	reheating
1	61.13 (12.65)	−3.63 (1.24)	5.56 (1.58)
		18.54 (1.28)	35.89 (4.96)
		32.65 (4.33)	45.37 (3.23)[a]
			53.00 (3.34)
2	16.38 (0.072)	4.86 (0.214)	4.22 (0.332)
	79.70 (0.152)	73.80 (0.048)	77.46 (0.045)
3	55.63 (0.174)	−8.06 (0.066)	−7.02 (0.358)
		51.54 (0.122)	53.63 (0.120)
4	43.03 (2.193)	−8.95 (0.909)	−8.53 (0.31)
		8.11 (0.057)	0.29 (0.982)
			11.39 (0.050)
5	50.49 (7.09)	18.83 (2.77)	−8.26 (0.082)
	139.85 (1.66)	24.85 (0.061)	22.88 (3.35)
			47.65 (0.107)
6	74.89 (8.09)	−8.23 (<0.05)	−8.18 (0.31)
		59.27 (0.074)	45.05 (5.50)[a]
			70.49 (5.79)
7	-	−2.82 (0.246)	−3.94 (0.303)

[a] Exothermic signals.

The enthalpy values for the different compounds were difficult to rationalize from a molecular point of view. The highest value was found for the standard compound (**1**) without regioisomerism. The presence of regioisomers in the synthesized compounds could be one reason for the lower enthalpy values and may also explain the behavior of **7**. However, other factors may influence the enthalpies because the other compounds have a similar content of regioisomers. The strength of the hydrogen bond was expected to be smaller and the enthalpies bigger for **5** and **6** compared with those of **3** and **4**.

On the basis of the DSC curves, the transition enthalpies were calculated for compounds **1**−**7**. The observed phase temperature transition and associated enthalpies are shown in Table 3. The enthalpy of the transition temperature (fusion) for the pure dodecane, a hydrocarbon with the same fatty chain length as compounds **1**−**7**, is ΔH= 8.8 kcal/mol,[21] which is larger than that obtained for the new compounds. The enthalpy values of **2**−**7** are also lower (ΔH= 8.4 kcal/mol) than that of nonhydrated lauroyl-lysophosphatidylethanolamine.[10] These results suggests than the disorder in the hydrocarbon chains in the melted bilayer of the new compounds is smaller than that in the pure liquid hydrocarbon and in the monoglyceride and lysophospholipid analogues.

3.3. SAXS Studies. The small-angle X-ray diffraction pattern of **1**−**6** showed a series of reflection peaks characteristic of lamellar packing on either side of the transitions of low temperature. The diffraction pattern of LAcY (**7**), however, did not show a peak but a wide band (see Figure 5A top), similar to the scattering curves obtained for weakly correlated lamellar phases. The DSC analysis did not show any transition for this compound. The maximum in the spectra, however, still corresponds to some characteristic distance present in the sample. For the rest of this discussion, the maximum in the scattering intensity will be treated as a lamellar peak. Therefore, the results corresponding to this compound should be taken only as approximate.

The repeat distances of these compounds at different temperatures are depicted in Figure 4. The plots show that the transition of these compounds in heating scans proceeds with the decrease of repeat spacing. Examination of *d* spacing in the first heating step suggests, for some compounds, the coexistence of a number of phases. The phase coexistence in these compounds would be related to the existence of both regioiso-

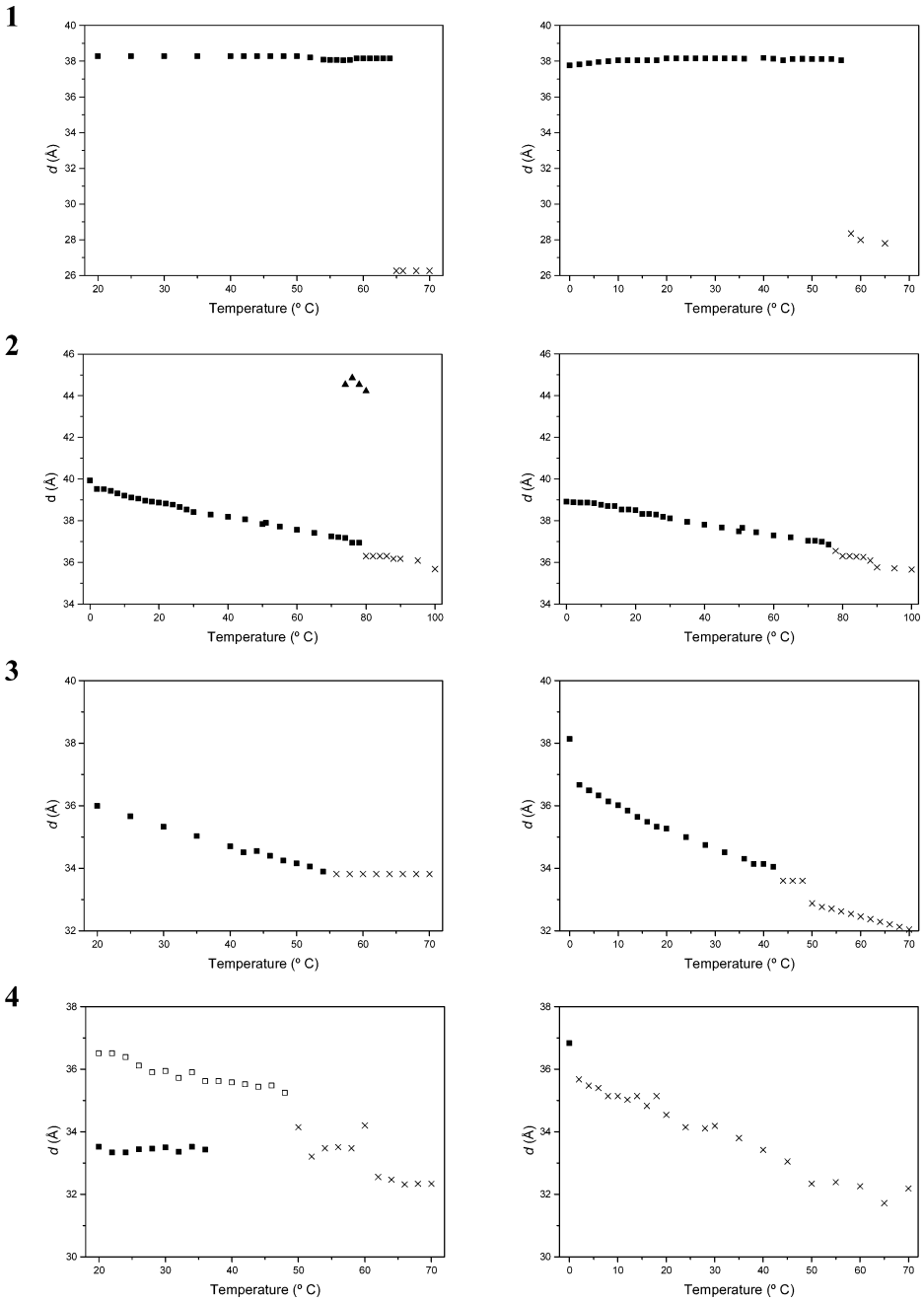

mers as well as to the diastereoisomers at different molar fraction, similarly to what was observed on isomeric mixtures of diacyl arginine-based surfactants.[22] However, because of some atmospheric water uptake during sample preparation (a maximum of about 0.5% as obtained from TGA analyses; this is about 1:4 water to surfactant molar ratio), we cannot discard the possible formation of different hydrates.

In **4**, **5**, and **6**, we attributed a lamellar structure to these coexisting phases, although only the first diffraction peak in the scattering curves can be clearly observed. The assignation was substantiated with previous results on isomeric mixtures of diacyl arginine-based surfactants, where several diffraction orders were detected for both lamellar coexisting phases.[22] In those cases, the shortest repeating distance phase was that stable at higher temperatures.

This behavior is opposite to that of what was observed with the arginine derivative (**2**). In this case, the repeating distance structure with $d \approx 37$ Å was stable at low temperature, whereas the higher temperature phase was that at $d \approx 44$ Å. This later peak increased intensity with the temperature. The shortest repeating distance peak at this temperature range broadens, indicating melting of the structure. At 82 °C, the long period peak suddenly disappears. It is difficult to interpret these observations. It is unclear how a coexisting lamellar phase would have such a different repeating distance. Moreover, other structures could be present. At 76 °C, an intermediate peak with a pattern compatible with a bicontinuous cubic structure was observed.

In the reheating process (Figure 4, right), the compounds exhibited a single lamellar phase in the X-ray diffraction pattern, suggesting complete miscibility between all the regioisomers in the different phases as was observed previously.[22] It is important to note that the scattering pattern of **5** differs from the others, In this case, a coexistence of a lamellar structure with a band at smaller q (bigger d) was present at all temperatures below fusion. This band was similar in shape to that characteristic of the melted state; however, its position did

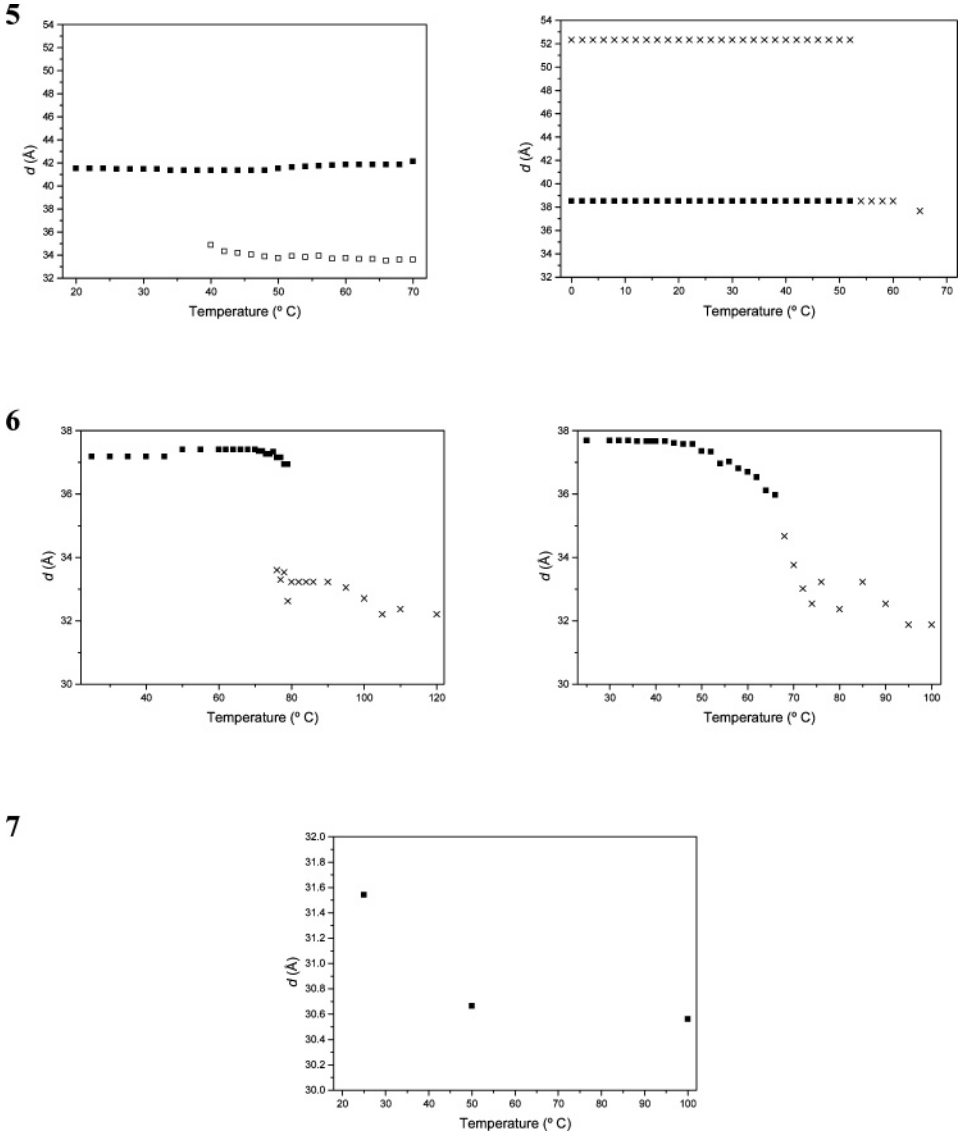

Figure 4. Temperature dependence of the X-ray spacing (d) of various phases observed for samples **1**−**7** in the heating mode. The identity of the phases is as follows: ■, □, lamellar phases (d_{001}); ×, melted; ▲, undefined phase. Left: first heating mode; right: second heating mode. In the case of compound **7**, only a heating mode was conducted. D spacing of the melted phases correspond to the maximum of the broad peak.

not correspond to the final melted pattern. In the case of **6**, the peak in this reheating scan is less defined than in the other cases.

The values of d spacing obtained from the reheating process will be used for the rest of the discussion because we hypothesize that this corresponds to the reproducible structure of the mixtures.

To obtain more information about the detailed structure of the compounds in the bilayer, the diffraction patterns of **1**−**7** were analyzed in terms of electron density profiles along the bilayer normal. The analyses were conducted in the gel phase of the reheating steps at low temperatures. We chose the gel state because more detailed structural information can be retrieved from the scattering curves because of higher structuring, only for **5** and **6**, the fit was carried out in the first heating mode, where sharp peaks were detected. Always, the second and third peaks in the scattering curves were absent or were extremely weak.

The classical approach to obtaining electron density profiles from diffraction curves consists of the Fourier synthesis.[23] However, this approach fails if only one or two orders of diffraction are present in the curves. In addition, because our experimental set up uses a slit collimated beam, desmearing of the experimental scattering profiles is needed before Fourier synthesis can be undertaken. The desmearing process enhances the noise and fails when diffraction peaks are present. Because of this, we have used the MCG method to fit our scattering curves. The MCG method[19] utilizes a modified Caillé theory structure factor in combination with a Gaussian model representation of the electron density profile such that it accounts also for the diffuse scattering between Bragg peaks. The method can retrieve useful structural information, even if only a few orders of diffraction are observed. The measured X-ray diffraction profiles of **1**−**7** in the reheating step at initial temperatures were fitted by using the MCG method (Figure 5A). Figure 5B shows a detailed experimental diffraction pattern of **3** at 0 °C. The solid line gives the best fit of the MCG model after smearing with the experimental beam geometry. The fit is in good agreement with the experimental data; the results for the fit parameters are given in Table 4. The quality of fit of compound **7** is noteworthy. We have to remark that the number of coherent scattering bilayers (2) and the Caillé parameter (the highest of the series) would correspond to a scarcely ordered phase that is coherent with the absence of birefringence. This could be a consequence of the presence of the aromatic ring in

TABLE 4: Fit Results for the Diffraction Patterns of Compounds 1−7 in the Reheating Step (compounds 1−5 0 °C, Compounds 6−7, 25 °C)

	compound						
fit parameter	1	2	3	4	5[a]	6[a]	7
d (Å)	37.5 ± 0.1	38.5 ± 0.04	36.4 ± 0.02	36.5 ± 0.05	40.5 ± 0.09	36.9 ± 0.05	33.6 ± 0.3
η_1	0.15 ± 0.01	0.09 ± 0.01	0.18 ± 0.01	0.13 ± 0.01	0.08 ± 0.01	0.15 ± 0.02	0.22 ± 0.01
N	13.4 ± 0.8	23.8 ± 1.5	58.9 ± 11.7	23.2 ± 2.2	8.0 ± 0.3	18.0 ± 1.4	2.00
σ_H (Å)	6.7 ± 0.6	7.7 ± 0.6	8.3 ± 0.3	4.9 ± 0.9	6.0 ± 0.7	10.0 ± 0.5	5.9 ± 0.7
σ_C (Å)	4.0 ± 9.8	6.5 ± 3.2	4.0 ± 0.5	8.1 ± 4.0	6.4 ± 1.1	4.6 ±0.5	13.5 ± 1.6
ρ_H (e/Å^3)	0.22 ± 0.01	0.13 ± 0.01	0.11 ± 0.01	0.12 ± 0.11	0.10 ± 0.02	0.18 ± 0.10	0.13 ± 0.03
ρ_C (e/Å$_3$)	−0.023 ± 0.01	−0.044 ± 0.01	−0.040 ± 0.01	−0.031 ± 0.01	−0.099 ± 0.01	−0.067 ± 0.01	−0.058 ± 0.01
N_{diff}	0	0	0	0	0	0	0
z_H (Å)	16.1 ± 0.4	12.0 ± 1.4	12.0 ± 0.2	12.2 ± 1.1	12.7 ± 0.2	12.0 ± 0.2	10.5 ± 0.6

[a] Diffraction patterns corresponding to the first heating mode.

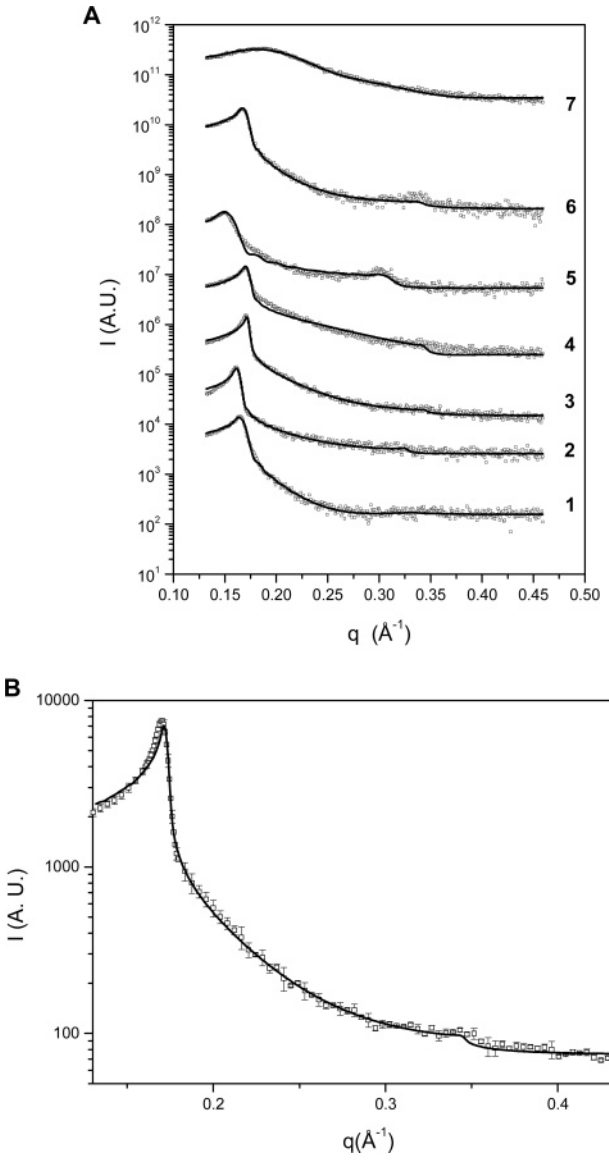

Figure 5. (A) Best fit of the MCG model (lines) to the diffraction pattern (square symbols) corresponding to the compounds **1**−**7**. (B) Enlarged view of the best fit of compound **3** at 0 °C, data with instrumental smearing and error bars.

the polar head, which can induce some favorable interaction with the hydrocarbon chains, leading to a weaker segregation of polar and nonpolar domains.

The fitting of the MCG model allowed for the calculation of the corresponding electronic profile (eqs 6−8). The electronic density profiles in arbitrary scale along the *z* axis are shown in Figure 6 for the seven compounds studied. The hydrophobic

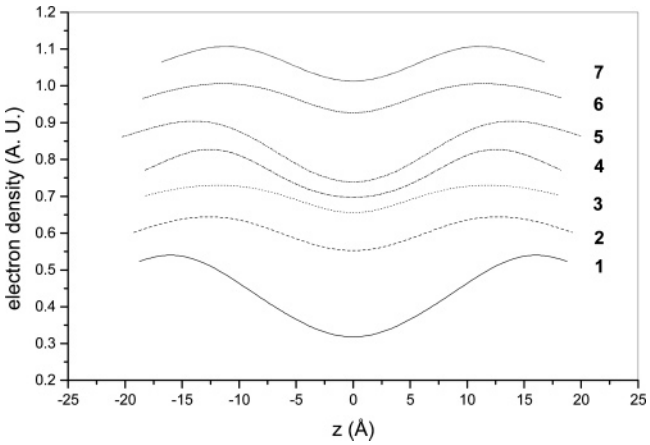

Figure 6. Electron density profiles of compounds **1**−**7** in the gel phases using the profile refined with the MCG model reported by Pabst et al.[19]

moieties corresponded to the low electronic density parts of the curves, and the polar heads were located in the high electronic density parts. Compound **1** showed density peaks located at 16 Å, while compounds **2**−**6** showed density peaks located at 12 Å. In the case of compound **7**, it is located at 11 Å. The low-density region in the center of the profiles corresponded to the acyl chains. In particular, the electron density trough in the center of the profiles indicated the localization of the low-density methyl groups, which was not detected in any cases. The electron density profiles derived showed that, for all the compounds, there was no terminal methyl dip in the center of the bilayer (Figure 6). This finding (lack of the terminal methyl trough), together with the narrow distance between the headgroups across the bilayer, is a consequence of the interdigitation of the acyl chains.[24−26] In the case of **1**, the absence of terminal methyl dip in the center of the bilayer would be correlated with a packing with nonspecific chain−chain interactions (melted chain) compatible with an α-phase. No reports about the electron density profile of monoglycerides are present in the literature.

The Gaussian electron density profiles for compounds **1**−**7** were set on an absolute scale. The scaling factor was computed by integrating the profile from the center to the border of the unit cell. This can be easily done because the electron density profile is given as an analytic function. The local order of the alkyl chain in the glycerol backbone was expected to be similar in the different molecular species. Hence, a comparison of the absolute electron density profiles would establish good correlation between the electron numbers on the headgroups in the bilayer. Unfortunately, the absolute electron density profiles of **1**−**7** did not show the expected similarities in the hydrophobic chains. Therefore, the differences with the headgroup electronic

TABLE 5: Derived Structural Parameters Derived Using the MCG Method

	1	2	3	4	5	6	7
d (Å)	37.5 ± 0.1	38.5 ± 0.04	36.4 ± 0.02	36.5±0.05	40.5 ± 0.09	36.9 ± 0.05	33.6 ± 0.3
d_C (Å)	13.4 ± 0.5	8.3 ± 2.1	8.9 ± 0.2	9.2± 1.7	9.0 ± 0.2	8.8 ± 0.3	7.4 ± 0.9
d_H (Å)	4.0 ± 0.5	10.9 ± 2.1	9.3 ± 0.2	9.1 ± 1.7	11.3 ± 0.2	9.7 ± 0.2	9.4 ± 0.8
A ($Å^2/_{molecule}$)	21.9 ± 0.6	38.8 ± 0.6	36.2 ± 0.6	35.2 ± 0.6	35.9 ± 0.6	36.8 ± 0.6	44.0 ± 0.6

densities may not be significant. We estimated the error in the scaling factor as bigger than 15%, similar to that found by other authors.[19,27]

The structural features found by electronic profiles were compatible with the structural parameters obtained for **1**−**7** derived from simple geometric relationships (MCG method) determining the area per molecule (A), the hydrocarbon chain length (d_C), and the headgroup size (d_H) (Table 5). In these compounds, the polar headgroup consists of the carbonyl group of the hydrocarbon chain of the amino acid, both bonded to the polar glycerol backbone via an ester linkage and the free hydroxyl of the glycerol backbone (see Figure 1 dotted sections). The nonpolar region of the molecules consists of the hydrocarbon chain without the carbonyl group. For **1**, the hydrophobic chain should be close packed, compatible with the minimum area per molecule for one C_{11} chain (21 $Å^2$).[28] As we can observe in Table 5, the experimental value (24.2 $Å^2$) was only slightly higher than this minimum value. Considering the hydrophobic volume of one C_{11} chain (325 $Å^3$), the hydrophobic length (d_C) would be close to 13.4 Å, which corresponds to a length shorter than a fully extended C_{11} (14.2 Å).[28] This difference in fatty chain length would be possible if (i) tilting respect to the bilayer normal, (ii) interdigitation of the fatty chain, or (iii) partial fusion is assumed. In the first case, the angle of tilting would be 16.4° with respect to the normal. In the second case, an incomplete interdigitation (14.2 Å/2)/13.4 Å, about 52%) may be assumed. In the third case, we must consider the structure of the packed 3-acyl-*sn*-glycerols obtained from the liquid isotropic.[15,20] In their α-phase, the chains are packed in a hexagonal lattice with nonspecific chain−chain interactions (melted chain). With this assumption, the difference in bilayer thickness would correlate with the introduction of one kink in the chain. It is described that the presence of a kink in a hydrocarbon chain produces a reduction of 1.25, being the measured reduction 0.8 Å.[29]

Taking **1** as a reference, the values for the other compounds were examined. Note that our calculations and discussion concerning these structures refer to the compounds that have undergone the complete melting and not the compounds directly obtained from the lyophilized process. For **2**−**7**, the area per molecule (A) was bigger, and hence, the molecular length was smaller. This is possible if tilting or interdigitation of the molecules is assumed. To shorten the bilayer thickness, the angle of tilting with respect to the bilayer normal would be from 51.4° for **5** to 62.6° for **7**, which would correspond to highly distorted structures. The observed molecular length was, however, consistent with the packing geometry of almost fully interdigitated hydrocarbon chains (80−90%) in an all-trans configuration because the bilayer thickness for these compounds was virtually identical to the sum of the full length of the C_{11} chain (14 Å)[28] and the overall thickness of the headgroup (10 Å) in the bilayer. This situation would be similar to that found in lysophospholipatidylcholine and lysophosphatidylethanolamine analogues in the gel phase.[30−33] The values of calculated headgroup length (d_H) in **2**−**7** were close to the overall thickness of phosphatidylcholine and phosphatidyletanolamine headgroups in the bilayer (≈ 10 Å).[19] In the case of **7**, the shorter hydrocarbon length compared with the other synthesized compounds could be explained in terms of further penetration of the hydrophobic tail in the relatively low polarity headgroup region. This could be responsible of the low correlation between lamellae. The broad structure of the peaks on its diffraction pattern would confirm this finding.

Conclusions

In this work, the molecular shape dependence of the bilayer packing was studied by means of polarized light microscopy (PLM), differential scanning calorimetry (DSC), and small-angle X-ray diffraction (SAXS). Studies of PLM and SAXS demonstrated that compounds **1**−**6** exhibited a thermotropic smectic phase. As a consequence, the substitution of the polar head did not engender any curvature into the system, which might lead to the formation of cubic or columnar phases. Interestingly, liquid crystalline phases were not found in the case of compound **7**. This could be due to an unsuitable hydrophilic/hydrophobic balance in the molecular structure.

Our X-ray data analysis demonstrated that, at low-temperature, compounds **2**−**7** form an interdigitated gel phase. The reason for the occurrence of such an interdigitated phase was the disproportion between the cross-section of the polar and apolar moieties, allowing two packing organizations: as globular structures with the apolar chains packed together in the interior of a sphere and the polar headgroup lying on the surface, or the packing in a lamellar arrangement with interdigitated chains, which now resembles the situation of a "normal" diacyl phospholipid. In both cases, a minimization of the hydrophobic free energy was guaranteed. Although for monoacyl glycerolipids the structure of lamellar phases has not been studied in detail, the existence of an interdigitated phase has been proven for 1-stearoyl-lysophospatidylcholine.[30,34] In accordance with the occurrence of such interdigitation is the known tendency of lysophospholipids to incorporate spontaneously into target cell membranes, thus again minimizing the Gibbs free energy.[30]

The present was the first approach in the application of the novel MCG model in the construction of the electron density profile of the gel phase in monoacyl compounds. This approach, in contrast to the conventional Fourier synthesis method, analyses both Bragg peaks and diffuse scattering. Therefore, we retrieved structural information, even if only a few orders of diffraction were observed. The electron density profiles and the fit of the diffraction pattern derived from the Fourier and MCG models have been compared.

Small-angle X-ray diffraction data in the gel phase revealed that the substitution of the polar head by different amino acid structures did not modify significantly the lamellar repeat distance with respect to the standard one. The observed area per molecule, however, was larger for the new compounds. This finding was consistent with their larger hydrophilic volumes. Consequently, interdigitation was promoted in the synthesized compounds (**2**−**7**).

Acknowledgment. This work was supported by the Spanish CYCIT, reference PPQ2003-01834 and MAT2004-04793-CO2. We are also grateful to J. Caelles and A. López for their assistance in the SAXS and DSC measurements, respectively.

References and Notes

(1) Reman, F. C.; Van Deenen, L. L. M. *Biochim. Biophys. Acta* **1967**, *137*, 592−594.
(2) Reman, F. C.; Demel, R. A.; de Gier, J.; Van Deenen, L. L. M.; Eibl, H.; Westphal, O. *Chem. Phys. Lipids* **1969**, *3*, 221−223.
(3) Gledhill, B. L.; Sawieki, W.; Croce, C. M.; Koprowski, H. *Exp. Cell Res*. **1972**, *73*, 33−40.
(4) Ferber, E. In *Biological Membranes*; Chapman, D., Wallach, D. F. H., Eds.; Academic Press: London, 1973; pp 221−252.
(5) Nuhn, P.; Brezesinski, G.; Dobner, B.; Förster, G.; Gutheil, M.; Dörfler, H. J. *Chem. Phys. Lipids* **1986**, *39*, 221−236.
(6) Lewis, R. N. A. H.; McElhaney, R. N.; Harper, P. E.; Turner, D. C.; Gruner, S. M. *Biophys. J.* **1994**, *66*, 1088−1103.
(7) Koynova, R.; Caffrey, M. *Biochim. Biophys. Acta* **1998**, *1376*, 91−145.
(8) Stafford, R. E.; Dennis, E. A. *Colloids Surf.* **1988**, *30*, 47−64.
(9) Arvidson, G.; Brentel, I.; Khan, A.; Lindblom, G.; Fontell, K. *Eur. J. Biochem*. **1985**, *152*, 753−759.
(10) Slater, J. L.; Huang, Ch.; Adams, R. G.; Levin, I. W. *Biophys. J.* **1989**, *56*, 243−252.
(11) Morán, C.; Infante, M. R.; Clapés, P. *J. Chem. Soc., Perkin Trans. 1* **2002**, 1124−1134.
(12) Morán, C.; Infante, M. R.; Clapés, P. *J. Chem. Soc., Perkin Trans. 1* **2001**, 2063−2070.
(13) Pérez, L.; Pinazo, A.; García, M. T.; Morán, M. C.; Infante, M. R. *New J. Chem*. **2004**, *28*, 1326−1334.
(14) Millqvist-Fureby, A.; Virto, C.; Adlercreutz, P.; Mattiason, B. *Biocatal. Biotransform*. **1996**, *14*, 89−111.
(15) Kodali, D. R.; Redgrave, T. G.; Small, D. M.; Atkinson, D. *Biochemistry* **1985**, *24*, 519−525.
(16) Malkin, T., Shurbagy, M. R. *J. Chem. Soc*. **1936**, 1628−1634.
(17) Larsson, K. *Ark. Kemi*. **1964**, *23*, 35−56.
(18) Persson, P. K. T. *Chem. Phys. Lipids* **1984**, *34*, 287−299.
(19) Pabst, G.; Rappolt, M.; Amenitsch, H.; Laggner, P. *Phys. Rev. E* **2000**, *62*, 4000−4009.
(20) Small, D. M. *Handbook of Lipids Research*; Plenum Press: New York and London, 1986; Vol. 4, Chapter 10, Glycerides, pp 345−394.
(21) Small, D. M. *Handbook of Lipids Research*; Plenum Press: New York and London, 1986; Vol. 4, Chapter 7, Aliphatic Hydrocarbons, pp 183−232.
(22) Morán, M. C.; Pinazo, A.; Clapés, P.; Pérez, L.; Infante, M. R.; Pons, R. *J. Phys. Chem. B* **2004**, *108*, 11080−11088.
(23) Wiener, M. C.; Suter, R. M.; Nagle, J. F. *Biophys. J.* **1989**, *55*, 315−325.
(24) McIntosh, T. J.; McDaniel, R. V.; Simon, S. A. *Biochim. Biophys. Acta* **1983**, *73*, 109−114.
(25) Ranck, J. L.; Keira, T.; Luzzati, V. *Biochim. Biophys. Acta* **1977**, *488*, 432−441.
(26) Nagle, J. F.; Tristram-Nagle, S. *Biochim. Biophys. Acta* **2000**, *1469*, 159−195.
(27) Petrache, H. I.; Tristam-Nagle, S.; Nagle, J. F. *Chem. Phys. Lipids* **1998**, *95*, 83−94.
(28) Tanford, C. *The Hydrophobic Effect Formation of Micelles and Biological Membranes*; John Wiley & Sons: New York, 1980; Chapter 6, Micelles, pp 42−59.
(29) Tanford, C. *The Hydrophobic Effect Formation of Micelles and Biological Membranes*; John Wiley & Sons: New York, 1980; Chapter 12, Motility and Order, pp 128−138.
(30) Hui, S. W.; Huang, C. *Biochemistry* **1986**, *25*, 1330−1335.
(31) Pascher, I.; Sundell, S.; Hauser, H. *J. Mol. Biol*. **1981**, *153*, 807−824.
(32) Hauser, H.; Pascher, I.; Pearson, R. H.; Sundell, S. *Biochim. Biophys. Acta* **1981**, *650*, 21−51.
(33) Hauser, H.; Pascher, I.; Sundell, S. *J. Mol. Biol*. **1980**, *137*, 249−264.
(34) Mattai, J.; Graham Shipley, G. *Biochim. Biophys. Acta* **1986**, *859*, 257−265.